

THEORY

Loop-to-Loop Magnetic Coupling Through a Circular Aperture in a Planar PEC Screen of Finite Thickness

FEIYAN ZHOU¹, YAN WU¹, ZHIXIN ZHANG¹², LINGYUN GU¹,
XUEFENG BAI¹, YAN WU¹, AND CHONGQING JIAO¹²

¹Beijing Key Laboratory of Distribution Transformer Energy-Saving Technology, China Electric Power Research Institute, Beijing 100192, China

²State Key Laboratory of Alternate Electrical Power System with Renewable Energy Source, North China Electric Power University, Beijing 102206, China

Corresponding author: Chongqing Jiao (cqjiao@ncepu.edu.cn)

This work was supported by Key technologies Research and application of primary and secondary deep integration with lean operation and maintenance of distribution switch based on Internet of things, under Grant 52130421000S.

ABSTRACT An analytical formulation for magnetic field penetration through a circular aperture in a thin perfect electric conductor (PEC) screen with finite-thickness is developed. Especially, we propose an analytical formula for the magnetic coupling between two circular loops separated by the screen and placed coaxially with the aperture. The formula is verified by finite element simulations and experimental data. The thickness effect is explained by the cut off attenuation of TE₀₁ mode in the aperture. The influences of loop-screen-loop distance and loop radius on the coupling intensity are also investigated.


INDEX TERMS Circular aperture, magnetic shielding, loop-to-loop magnetic coupling, magnetic quadrupole, mutual inductance.

I. INTRODUCTION

Shielding of low frequency magnetic field using metal screens (enclosure, sheets, wire meshes) has been important for many decades and is now even more indispensable with the burgeoning number of RF transmitters and sensitive devices of all types [1], [2], [3], [4], [5], [6]. Frequently, a screen has to contain apertures or slots for ventilation or cabling purposes. These clearly may reduce the shielding performance. Previous researches show that apertures are the primary path for magnetic field leakage at higher frequencies, and by contrast magnetic diffusion through metal sheet is dominant at lower frequencies [7], [8], [9], [10]. In term of analytical formulation of magnetic field leakage through an aperture in a planar sheet, Bethe's small aperture coupling theory is widely adopted [7], [11], [12]. Where, the aperture is modelled as a magnetic dipole with its moment proportional to the tangential component of external applied magnetic field. However, this treatment requires the premise that the applied field distributes uniformly across the

aperture surface. For example, when the emitting loop and the receiving loop are coplanar and perpendicular to the infinite slotted conducting plate [13], the tangential component of the magnetic field in the slit is considered to be uniform and Bethe's small aperture coupling theory can be applied.

For the case where the loops are coaxial with each other and parallel to the solid shielding planar plate, Ref. 14 studies the effects of loop radius and loop-to-loop distance for the infinite screen; and Ref. 15 studies the loop-to-loop coupling in the case of a shielding plate with limited radius. In a recent paper [16], a circular aperture on the screen is investigated where the applied field is produced by a circular current loop placed coaxially with a circular aperture. Then the tangential magnetic field on the aperture surface will be nonuniform and omnidirectional. Especially, the analytical expression for the longitudinal component of the shielded magnetic field is obtained if only the emitting loop radius or the loop-to-aperture distance is much larger than the radius of the aperture. However, this research has two limitations. The first one is the lack of analytical formula for the loop-to-loop coupling. This requires an integration of magnetic flux density through the receiving loop. However, a check of the

The associate editor coordinating the review of this manuscript and approving it for publication was Luyu Zhao .

accurate flux density expression (Eq. 25, Ref.16) supports that its integration can not be solved analytically. The second is that the thickness of the screen is negligible, which leads to the overestimate of the leakage field.

This letter aims to relax the two limitations. First, noting that the field distribution far from the aperture (Eq. 28, Ref. 16) is similar to that produced by a quadrupole, an analytical formula of the magnetic vector potential is derived. Then, the formula for the integration can be obtained easily. Second, the thickness is considered with the attenuation effect of waveguide below cut off, which results in an overall exponential decay of the shielded field. Further, the effects of changing the receiving loop radius and moving the screen longitudinally are analyzed. Such analysis is of practical interest. In addition, we show that the tangential component of magnetic field on the illuminated side of the aperture can be approximated as the unshielded field, which can be applied to evidently reduce the computing time and memory in numerical simulation.

II. MODEL AND THEORY

As shown in the Fig. 1, a circular aperture of radius a is drilled in a planar PEC screen of infinite extension and with thickness t . The emitting loop, placed coaxially with the aperture, has a radius r_1 and carries a time harmonic current I with frequency f . A receiving loop with the radius r_2 is coaxial with the aperture, too. The distance from the upper surface of the screen to the emitting loop is z_1 , and to the receiving loop is z_2 . The coordinate origin is at the center of the upper surface of the aperture and the z -axis is coincident with the axis of the aperture.

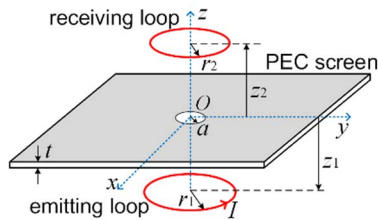


FIGURE 1. Low-frequency magnetic field generated by the emitting loop penetrates a circular aperture in an infinite planar PEC screen of thickness t .

It should be noted that the analytical model should meet quasi-static conditions: the sizes of the two loops and the loop-to-loop distance are electrically small relative to the free space wavelength λ (size $< \lambda/2\pi$). In practice, the sizes are usually less than 1 m, and hence up to 30 MHz ($\lambda = 10$ m) the configuration is still electrically small. Then, the above magnetic shielding problem can be treated well using quasi-static formulation. Especially, when the thickness t tends to zero and the aperture is small ($a < r_1$ or $a < z_1$), an analytical formula for magnetic field on the z -axis ($z > 0$) is proposed in [16],

$$H_{sz}(0, z) = \frac{ar_1^2 z_1}{\pi (r_1^2 + z_1^2)^{5/2}} \left[\frac{1}{1 + (a/z)^2} - 3 \frac{\arctan(a/z)}{a/z} + 2 \right] \quad (1)$$

Further, if $z > 2a$, Eq. 1 is approximated as

$$H_{sz}(0, z) = (2/5\pi) a^5 I r_1^2 z_1 (r_1^2 + z_1^2)^{-5/2} z^{-4} \quad (2)$$

Here, equation (2) is explained quantitatively as the results of a magnetic quadrupole placed in the aperture center (the coordinate origin), as shown in the Fig. 2. Wherein, the magnetic quadrupole consists of two close magnetic dipoles with the same moment m but opposite directions ($+z$ and $-z$). The spacing h of the two dipoles tends to zero, while the product of m and h keeps unchanged.

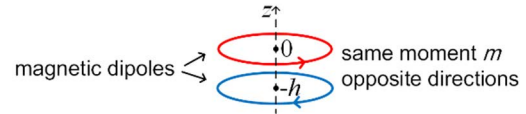


FIGURE 2. Model of a magnetic quadrupole consisting of two close magnetic dipoles with the same moment m but opposite directions.

It is easy to prove, if we let

$$mh = (4/15) a^5 I r_1^2 z_1 (r_1^2 + z_1^2)^{-5/2} \quad (3)$$

then the field generated by the quadrupole will be identical to that expressed by Eq. 2. In other words, the leakage field is equivalent to the free space field of the quadrupole. Then, the corresponding magnetic field intensity and vector potential can be written in cylindrical coordinator system (ρ, ϕ, z) as

$$\begin{aligned} \mathbf{H}_s &= H_{sz} \mathbf{e}_z + H_{s\rho} \mathbf{e}_\rho \\ &= \frac{(6z^3 - 9z\rho^2) mh}{4\pi (z^2 + \rho^2)^{7/2}} \mathbf{e}_z + \frac{(12z\rho z^2 - 3\rho^3) mh}{4\pi (z^2 + \rho^2)^{7/2}} \mathbf{e}_\rho, z > 0 \end{aligned} \quad (4)$$

$$\mathbf{A}_s = A_{s\phi} \mathbf{e}_\phi = \frac{3\mu_0 z \rho mh}{4\pi (\rho^2 + z^2)^{5/2}} \mathbf{e}_\phi, z > 0 \quad (5)$$

For a receiving loop of radius r_2 and with a distance z_2 from the screen, the magnetic flux through this loop is

$$\Phi_s = 2\pi \rho A_{s\phi} |_{\rho=r_2} = \frac{2\mu_0 a^5 I r_1^2 z_1 r_2^2 z_2}{5 (r_1^2 + z_1^2)^{5/2} (r_2^2 + z_2^2)^{5/2}} \quad (6)$$

Attention now turns to the screen thickness t . In the aperture, the field will experience exponential attenuation like $e^{-\alpha t}$ resulted from the effect of waveguide below cutoff. Considering the configuration is axisymmetric and transverse-electric, the attenuation coefficient is related to the TE_{0n} modes ($n = 1, 2, 3, \dots$). In order to obtain a simple approximate analytical formula for calculating shielding effectiveness (SE), we overestimated the leakage field and select the TE₀₁ mode with the weakest attenuation among them to describe the shielded field [17], [18], [19]. Then, the attenuation coefficient α is expressed as

$$\alpha = \frac{3.832}{a} \sqrt{1 - \left(\frac{2\pi af}{3.832c} \right)^2} \approx \frac{3.832}{a} \quad (7)$$

where, c is the speed of light in free space.

With this attenuation considered, both the magnetic field (4) and magnetic flux (6) should be modified as

$$\mathbf{H}_s \rightarrow \mathbf{H}_s e^{-3.832t/a}, \Phi_s \rightarrow \Phi_s e^{-3.832t/a} \quad (8)$$

The SE of the screen is usually defined as the ratio of the induced voltage in the receiving loop with the screen absent to that with the screen in presence. This voltage based on definition can be replaced equivalently with mutual inductance between the two loops like

$$SE = 20 \log (M_0/M_s) \quad (9)$$

wherein, M_s refers to the mutual inductance with the screen present and is calculated as Φ_s/I . M_0 denotes the mutual inductance with the screen absent, and its expression is well known [20].

In practice, a screen is usually made of metal material like aluminum, copper and steel. These screens can behavior well like a PEC screen when magnetic diffusion effect is weaker than aperture leakage effect, which typically happens when frequency is above tens of or hundreds of kHz, depending on the concrete geometry and material parameter [16].

III. VALIDATION

First, the field point on the z -axis is considered. Here, the loop-to-point SE can be calculated by the ratio of the magnetic field intensity observed at a given position with the enclosure removed to that observed at the same point with the enclosure loaded. The SE- z/a curves are plotted in the Fig. 3 for different r_1/a , z_1/a , and t/a . The calculated results are obtained using the magnetic field in Eq. 8. Meanwhile, the simulation results with $f = 0$ Hz from a 2D axis-symmetrical finite-element method (FEM) model built in the COMSOL are also provided for comparison. It should be noted that under the PEC boundary condition (the normal magnetic field component on the surface of the PEC screen is zero), the results are frequency-independent within the quasi-static range [16].

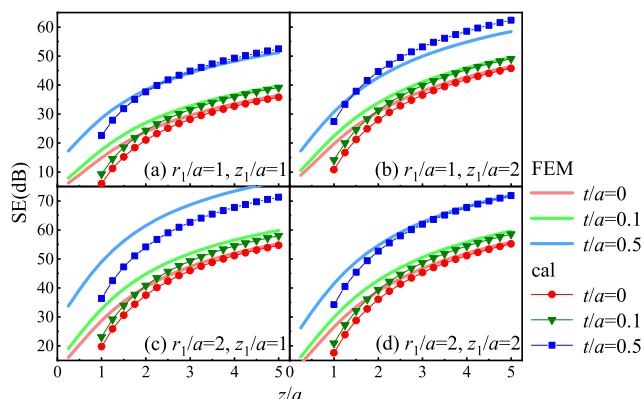


FIGURE 3. The SE- z/a curves with different r_1/a and z_1/a ($a = 1$ cm). “FEM” and “cal” correspond to the SE results obtained from the FEM simulation and theoretical calculation, respectively.

The results show that the approximate analytical formula (8) is in good agreement with the FEM results when

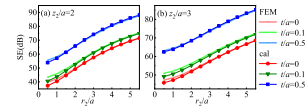


FIGURE 4. The SE- r_2/a curves for different z_2/a with $r_1/a = 2$ and $z_1/a = 2$.

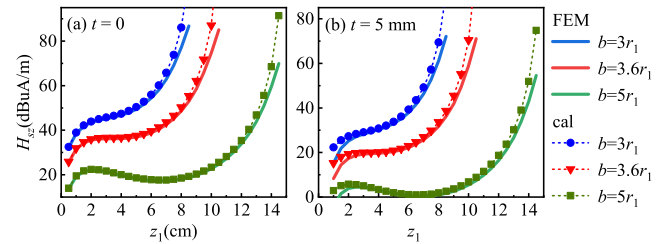


FIGURE 5. Curves of calculated and FEM simulated H_{sz} with $r_1 = 3$ cm, $a = 1$ cm, and $I = 1$ A.

$r_1/a > 2$, $z_1/a > 2$, and $z/a > 2$. However, beyond the range of this condition, it cannot be said that the FEM results under all parameters are inconsistent with the analytical results. For example, when $r_1/a = 1$, $z_1/a = 1$, and $z/a > 2$, the calculation results also agree well with the FEM. Therefore, we set the conditions of “ $r_1/a > 2$, $z_1/a > 2$, and $z/a > 2$ ” as a conservative description of the scope of application for the analytical formula.

Second, the loop-to-loop SE is considered. Combined with the above analysis, Fig. 4 shows the calculated (Eq. 9) and FEM-simulated (PEC boundary condition and $f = 0$ Hz) SE- r_2/a curves with $r_1/a = 2$ and $z_1/a = 2$. It can be seen that the calculation results of the loop-to-loop SE formula are in good agreement with the FEM simulation for different t/a in the case of $z_2/a > 2$.

IV. APPLICATIONS

A. EFFECT OF THE LOOP-TO-SCREEN DISTANCE

For an infinite solid planar conducting screen, the emitting-loop-to-screen distance z_1 has no effect on the SE under the premise that the loop-to-loop distance b ($b = z_1 + z_2$) is fixed [1]. However, for the perforated planar PEC screen, z_1 has an impact.

When the observation point is on the z -axis, the shielded field (2) can be expressed as

$$H_{sz} = \frac{2r_1^2 a^5 I}{5\pi} \frac{z_1}{(r_1^2 + z_1^2)^{5/2} (b - z_1)^4} e^{-3.832t/a} \quad (10)$$

Take the derivative of (10) and we get the conclusion that if $0 < b \leq 3.6r_1$, H_{sz} increases with z_1 ; if $b > 3.6r_1$, with the increase of z_1 , the trend of H_{sz} is to increase first, then decrease, and finally increase. In general, the magnetic field increases as the screen moves closer to the receiving side. The magnetic field curves changing with z_1 under various b are shown in the Fig. 5.

The calculated H_{sz} from (10) is in good agreement with the FEM results in the range of $z_1 > 2a$ and $z_2 > 2a$. It can

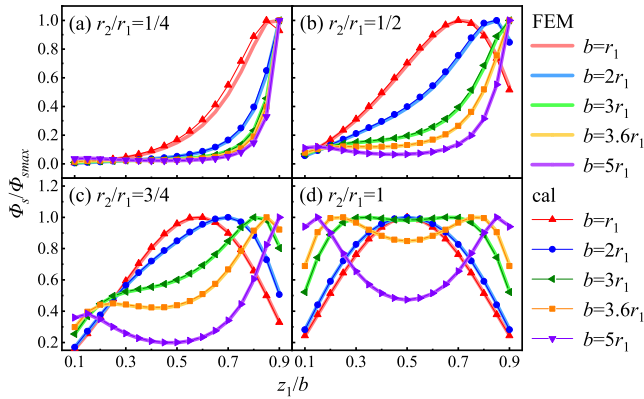


FIGURE 6. Curves of normalized Φ_s with $r_1 = 8$ cm, $a = 1$ cm, and $I = 1$ A.

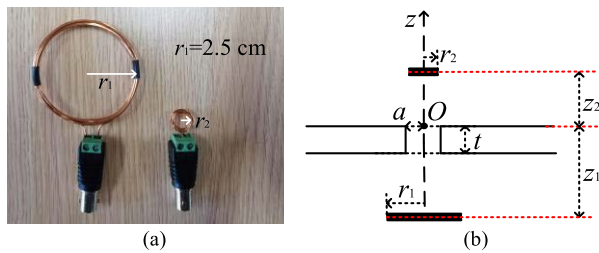


FIGURE 7. Experimental configuration: (a) the emitting and receiving loops used in the measurement; (b) the definition of z_1 and z_2 .

be seen that the trend of H_{sz} is consistent with the above conclusions. For larger loop-to-loop distance, the range of distances in which “cal” and “FEM” are consistent also expands. Practically, the distance between rings is often large, so the analysis results are consistent with FEM in a wide range.

For the loop-to-loop situation, we calculate the magnetic flux Φ_s (Eq. 6) through the receiving loop with different loop-to-loop distance in the Fig. 6, and the data has been normalized for a more intuitive display. It shows that when $r_2/r_1 = 1/4$ and $1/2$, Φ_s generally increases with the screen moving close to the receiving loop. In the case of $r_1 = r_2$ as (d) shows, the curves of Φ_s are symmetrical. When the loop-to-loop distance is relatively large such as $b = 5r_1$, the screen in the middle position can produce the highest SE; and when $b < 3r_1$, the screen in the middle produces the lowest SE.

Some experiments were carried out to investigate the effect of the emitting-loop-to-screen distance on SE when the loop-to-loop distance is fixed. The SE of a perforated finite conductivity conductor (FCC) screen ($1\text{ m} \times 1\text{ m}$, 3.8×10^7 S/m, $t = 1$ mm, and $a = 2$ cm) is measured by the handmade loops shown in Fig. 7(a) with $f = 300$ kHz. The emitting loop (10 turns) is 2.5 cm in loop radius, 2 mm in wire radius and the receiving loop (15 turns) is 0.5 cm in loop radius, 1 mm in wire radius. Here, we define z_1 and z_2 as the distance from the upper surface of the screen to the middle position of the emitting and receiving loops respectively as shown in Fig. 7(b).

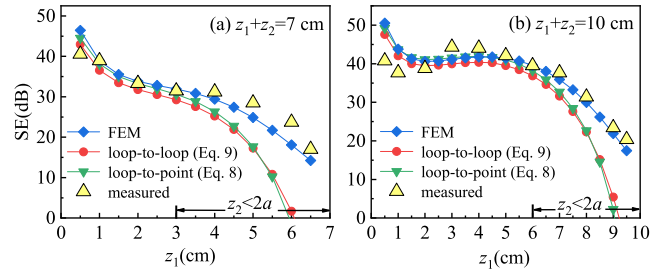


FIGURE 8. Curves of SE- z_1 at various z_1+z_2 with $t = 1$ mm, $a = 2$ cm. “FEM” and “measured” denote the FEM simulated SE and the experimentally measured SE; “loop-to-loop (Eq. 6)” and “loop-to-point (Eq. 2)” are the SE results calculated using Eqs. 6 and 2, respectively.

Further, some measurement results are displayed for $z_1 + z_2 = 7$ cm (Fig. 8(a)) and 10 cm (Fig. 8(b)). We also calculated the SE of the loop-to-loop model (using Eq. 9) and the loop-to-point model (using Eq. 8 with $\rho = 0$).

When the radius of the receiving loop is relatively small, the loop-to-point SE and loop-to-loop SE agree well. The measured and FEM simulated SEs are in good agreement with each other and generally decrease with increasing z_1 . The calculated results are no longer accurate when $z_2 < 2a$. For example, as z_2 approaches 0 and the shielded field in Eqs. 2 and 6 approaches infinity, which leads to wrong SE results (close to 0 or even negative).

It should be noted that the loops in Fig. 7 are different from that used in the Ref.16. Where the emitting loop has a metal frame, which makes it difficult to determine the equivalent radius of the practical loop when it is treated as an equivalent ideal loop. In contrast, the handmade loops have relatively small wire radius and there is no attached frame structure, which can reduce the uncertainty in the parameters (r_1 , r_2 , z_1 , and z_2). Due to this improvement, the present experimental configuration has better agreement with our theoretical model.

It is also worth noting that the screen can be regard as PEC with $f = 300$ kHz. The reason is that the same FCC screen has experimentally behaved like PEC even for $f = 100$ kHz (see Fig. 6(b) in Ref.16).

B. THE MAXIMUM COUPLING RADIUS

Here, we investigate the effect of the receiving loop radius r_2 on the coupling (mutual inductance M_s) of the two loops. Keeping other parameter unchanged, the maximum coupling occurs when

$$r_2' = \sqrt{2/3z_2} \approx 0.82z_2 \quad (11)$$

Besides, (11) can also be obtained by solving the r_2' when the direction of H_{sz} changes, that is, to find the zero point of H_{sz} in (4). Equation (11) was experimentally verified using the receiving loops with different radius in the Fig. 9. Considering that the mutual inductance is proportional to the induced voltage, the coupling is studied by testing the induced voltage in the experiment with $r_1 = 6$ cm, $z_1 = 5$ cm, $a = 2$ cm, $t = 1$ mm, and $f = 300$ kHz.

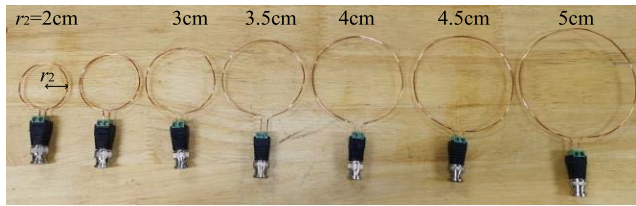


FIGURE 9. Receiving loops with different radius: $r_2 = 2$ cm, 2.5 cm, 3 cm, 3.5 cm, 4 cm, 4.5 cm, 5 cm (from the left to the right).

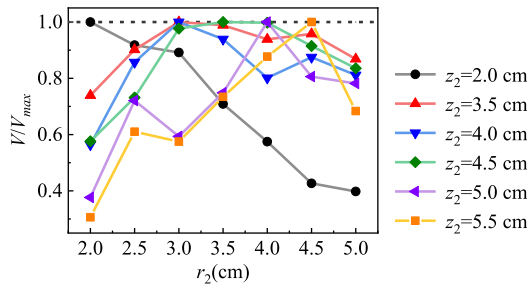


FIGURE 10. The normalized voltage received by the loops with different radius.

TABLE 1. Comparison between the experimental and the calculated results about the maximum coupling radius.

z_2 (cm)	2.0	3.5	4.0	4.5	5.0	5.5
r_{2-m} (cm)	< 2	3	3	3.5	4	4.5
r_2' (cm)	1.64	2.87	3.28	3.69	4.10	4.51

The normalized induced voltage curves are shown in the Fig. 10. The experimental maximum coupling radius r_{2-m} and the theoretical result r_2' (Eq. 11) under different z_2 are listed in the Tab. 1. We can see that r_{2-m} is basically consistent with r_2' .

C. BOUNDARY CONDITIONS FOR THE APERTURE SURFACE

When the screen thickness is equal to zero, the tangential component of the magnetic field on the aperture surface is equal to that produced by the current loop alone without the screen [16]. For the PEC screen with a thickness t ($t \neq 0$), we would like to investigate whether the tangential magnetic field $H_{a\rho}$ of the aperture surface on the illuminated side is still equal to the unshielded. Therefore, the illuminated magnetic field of a screen with different thickness and the unshielded field in free space are calculated using FEM simulation. The results are shown in the Fig. 11 and the ratio of the unshielded to the shielded field is within the range 0.85–0.99 (–1.41 to –0.09 dB). This shows that the tangential component on the illuminated side of the aperture can be approximated as the unshielded one.

Using the unshielded field as a boundary condition of the aperture surface on the illuminated side, the field H_{sz}' and H_{sp}' on the non-illuminated side is calculate by the FEM simulations. The FEM results H_{sz} and H_{sp} are from the original

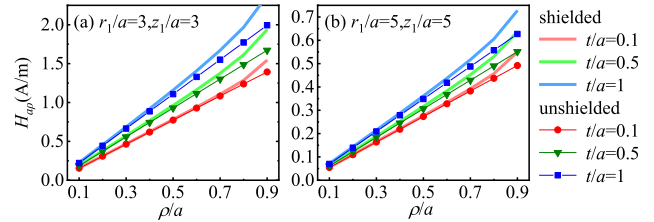


FIGURE 11. FEM results of the tangential magnetic field $H_{a\rho}$ ($a = 1$ cm, $I = 1$ A). Where, “shielded” and “unshielded” represent the shielded field on the illuminated aperture surface side and the unshielded field in free space.

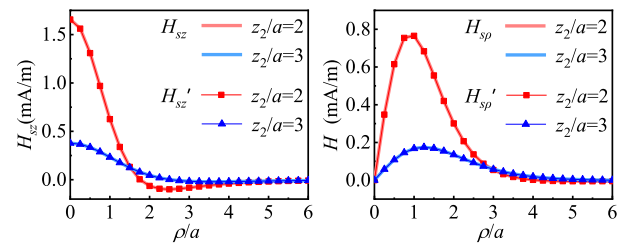


FIGURE 12. Curves of FEM simulation magnetic field on the non-illuminated side of a perforated PEC screen ($a = 1$ cm, $I = 1$ A, $r_1/a = 3$, $z_1/a = 3$, and $t/a = 0.5$).

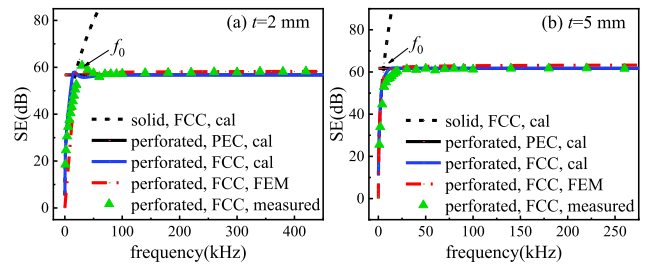


FIGURE 13. Comparisons of the loop-to-loop SE for the solid FCC, perforated PEC and perforated FCC screens ($r_1 = 6$ cm, $z_1 = 5$ cm, $r_2 = 2.5$ cm, $z_2 = 5$ cm, $a = 2$ cm). Where, “solid, FCC, cal” denotes the calculated SE of a solid FCC screen; “perforated, PEC, cal” refers to the calculated SE of a perforated PEC screen; “perforated, FCC, cal”, “perforated, FCC, FEM” and “perforated, FCC, measured” correspond to the SE results of a perforated FCC screen obtained from calculation, FEM simulation and measurement respectively.

model of perforated PEC screen in the Fig. 1. Fig. 12 shows that using the boundary condition that the tangential magnetic field on the illuminated aperture surface is equal to the field without shielding can produce the same field with the original model, through which the range of field domain can be cut down.

D. APPLICATION TO THE SCREEN WITH A FINITE CONDUCTIVITY

Here, the dependence of SE on frequency is investigated by measurements and FEM simulations. Meanwhile, the calculated SE for perforated FCC screen is obtained by the superposition principle: the field corresponding to the perforated FCC screen is the sum of the field for the solid FCC screen and the perforated PEC screen [7], [16]. The SE of a solid

FCC screen is calculated using the ratio of magnetic flux in [21], and that of the perforated PEC screen is calculated by Eq. 9. SE of the perforated FCC screens with different thicknesses ($t = 2$ and 5 mm) is also measured by the SE test-bench setup [16] and simulated using FEM software.

For the perforated FCC screen, the SE versus frequency exhibits two-stage behavior: it increases when $f < f_0$ (diffusion effect) but is nearly unchanged when $f > f_0$ (aperture effect). Where, f_0 is the intersection frequency of the solid FCC screen curve and the perforated PEC screen curve. From Fig. 13, f_0 is about 15 kHz and 10 kHz for $t = 2$ and 5 mm, respectively. It can be seen that f_0 is smaller with larger thickness.

V. CONCLUSION

The leakage magnetic field from a circular aperture in a PEC screen, when excited by a circular current loop placed coaxially with the aperture, is expressed analytically using equivalent magnetic quadrupole. An analytical formula is proposed to predict the magnetic coupling between two circular loops separated by the PEC screen and placed coaxially with the aperture. Comparisons with FEM simulations show the field expression is applicable for observation points beyond two times of aperture radius away from the aperture. Effect of the screen thickness is explained by the exponential attenuation of TE₀₁ mode below cut off in the aperture. With fixed loop-to-loop distance, the SE reduces with the screen moving close to the receiving loop for smaller receiving loop. By contrast, for larger receiving loop and loop-to-loop distance, the SE is highest when the screen is in the middle of the two loops. Keeping other parameter unchanged, the maximum coupling occurs when the receiving loop radius equals 0.82 times of the receiving-loop-to-screen distance. The tangential component of magnetic field on the illuminated side of the aperture can be approximated as the unshielded field, and hence in numerical simulation the range of field domain can be cut down.

REFERENCES

- [1] S. Celozzi, R. Araneo, and G. Lovat, *Electromagnetic Shielding*. Hoboken, NJ, USA: Wiley, 2008.
- [2] Y. Zhou, L. Zhang, S. Xiu, and W. Hao, "Design and analysis of platform shielding for wireless charging tram," *IEEE Access*, vol. 7, pp. 129443–129451, 2019.
- [3] A. Z. E. D. Mohamed, H. G. Zaini, O. E. Gouda, and S. S. M. Ghoneim, "Mitigation of magnetic flux density of underground power cable and its conductor temperature based on FEM," *IEEE Access*, vol. 9, pp. 146592–146602, 2021.
- [4] J. Kim and S. Ahn, "Dual loop reactive shield application of wireless power transfer system for leakage magnetic field reduction and efficiency enhancement," *IEEE Access*, vol. 9, pp. 118307–118323, 2021.
- [5] A. Hirata, Y. Diao, T. Onishi, K. Sasaki, S. Ahn, D. Colombi, V. De Santis, I. Laakso, L. Giaccone, J. Wout, E. Rashed, W. Kainz, and J. Chen, "Assessment of human exposure to electromagnetic fields: Review and future directions," *IEEE Trans. Electromagn. Compat.*, vol. 63, no. 5, pp. 1619–1630, Oct. 2021.
- [6] G. Lovat, P. Burghignoli, R. Araneo, E. Stracqualursi, and S. Celozzi, "Analytical evaluation of the low-frequency magnetic shielding of thin planar magnetic and conductive screens," *IEEE Trans. Electromagn. Compat.*, vol. 63, no. 1, pp. 308–312, Feb. 2021.
- [7] A. Frikha, M. Bensetti, F. Duval, N. Benjelloun, F. Lafon, and L. Pichon, "A new methodology to predict the magnetic shielding effectiveness of enclosures at low frequency in the near field," *IEEE Trans. Magn.*, vol. 51, no. 3, pp. 1–4, Mar. 2015.
- [8] X. Yang, Z. Zhang, F. Ning, C. Jiao, and L. Chen, "Shielding effectiveness analysis of the conducting spherical shell with a circular aperture against low frequency magnetic fields," *IEEE Access*, vol. 8, pp. 79844–79850, 2020.
- [9] W. Bai, F. Ning, X. Yang, C. Jiao, and L. Chen, "Low frequency magnetic shielding effectiveness of a conducting plate with periodic apertures," *IEEE Trans. Electromagn. Compat.*, vol. 63, no. 1, pp. 30–37, Feb. 2021.
- [10] S.-I. Matsuzawa, T. Kojima, K. Mizuno, K. Kagawa, and A. Wakamatsu, "Electromagnetic simulation of low-frequency magnetic shielding of a welded steel plate," *IEEE Trans. Electromagn. Compat.*, vol. 63, no. 6, pp. 1896–1903, Dec. 2021.
- [11] H. A. Bethe, "Theory of diffraction by small holes," *Phys. Rev. Lett.*, vol. 66, nos. 7–8, pp. 163–182, Oct. 1944.
- [12] H. H. Park, "Analytic magnetic shielding effectiveness of multiple long slots on a metal plate using rectangular loops," *IEEE Trans. Electromagn. Compat.*, vol. 62, no. 5, pp. 1971–1979, Oct. 2020.
- [13] H. H. Park and J. W. Lee, "Analytical magnetic shielding calculation of a slotted conducting plate between coplanar circular loops," *IEEE Trans. Electromagn. Compat.*, vol. 64, no. 2, pp. 378–385, Apr. 2022.
- [14] D. Qin and C. Jiao, "Low-frequency magnetic shielding of planar screens: Effects of loop radius and loop-to-loop distance," *IEEE Trans. Electromagn. Compat.*, vol. 64, no. 2, pp. 367–377, Apr. 2022.
- [15] C. Jiao, X. Yang, and L. Qi, "Low-frequency magnetic shielding of a perfectly electric conducting circular disk: Approximately analytical formulation considering radius of emitting loop," *IEEE Trans. Electromagn. Compat.*, vol. 64, no. 3, pp. 897–901, Jun. 2022.
- [16] Z. Zhang, X. Yang, C. Jiao, Y. Yang, and J. Wang, "Analytical model for low-frequency magnetic field penetration through a circular aperture on a perfect electric conductor plate," *IEEE Trans. Electromagn. Compat.*, vol. 63, no. 5, pp. 1599–1604, Oct. 2021.
- [17] R. B. Schulz, V. C. Plantz, and D. R. Brush, "Shielding theory and practice," *IEEE Trans. Electromagn. Compat.*, vol. EC-30, no. 3, pp. 187–201, Aug. 1988.
- [18] Y. S. Lee and H. J. Eom, "Field penetration into a circular aperture pierced by a long cylinder," *IEEE Trans. Antennas Propag.*, vol. 58, no. 11, pp. 3734–3737, Nov. 2010.
- [19] C. R. Paul, *Introduction to Electromagnetic Compatibility*, 2nd ed. New York, NY, USA: Wiley, 1966, Sec. 10.5.
- [20] C. R. Paul, *Inductance: Loop and Particle*. Hoboken, NJ, USA: Wiley, 2010.
- [21] J. R. Moser, "Low-frequency shielding of a circular loop electromagnetic field source," *IEEE Trans. Electromagn. Compat.*, vol. EC-9, no. 1, pp. 6–18, Mar. 1967.



FEIYAN ZHOU was born in Hebei, China, in 1995. She received the B.E. and M.E. degrees in electrical engineering from Xi'an Jiaotong University, Xi'an, China, in 2017 and 2020, respectively. She is currently working with the China Electric Power Research Institute. Her research interests include power distribution automation, fault detection, and electromagnetic compatibility.



YAN WU was born in Nanyang, Henan, China, in 1982. She graduated from North China Electric Power University, in 2010. She received the master's degree in electromagnetic field and microwave technology.

Since 2010, she has been engaging in the research of power distribution system and equipment test technology at the Power Distribution Technology Center, China Electric Power Research Institute.



ZHIXIN ZHANG was born in Jilin, China, in 1997. She received the B.E. and M.E. degrees in electrical engineering and automation from North China Electric Power University (NCEPU), Beijing, China, in 2019 and 2022, respectively. Her research interests include electromagnetic shielding techniques and electromagnet compatibility in power systems.



YAN WU received the bachelor's degree in electrical engineering from Shenyang Agricultural University, Shenyang, China, in 2020. She is currently with the China Electric Power Research Institute. Her research interests include distribution automation and fault diagnosis of intelligent distribution networks.



LINGYUN GU received the M.A.Eng. degree in materials science from North China Electric Power University, Beijing, China, in 2016. He is currently working with the China Electric Power Research Institute. His research interests include test and detection technology of distribution systems and medium and low voltage complete sets of devices.



XUEFENG BAI received the master's degree in electrical power system and automation from China Agricultural University, Beijing, China, in 2008. He is currently working with the China Electric Power Research Institute. His research interests include automatic detection technology of medium and low voltage distribution equipment.



CHONGQING JIAO was born in Hubei, China. He received the B.Sc. degree in geophysics from the Chinese University of Geosciences, Wuhan, China, in 2002, and the Ph.D. degree in physical electronics from the Institute of Electronics, Chinese Academy of Sciences, Beijing, China, in 2007. He is currently an Associate Professor of electrical and electronic engineering with North China Electric Power University, Beijing. His research interests include electromagnetic theory and applications and the EMC in power systems.

...